Analysis of High-Energy Tailing in TlBr Detectors

Sean O'Neal, Zhong He, *Senior Member*, and Charles Leak

***Abstract*—TlBr is an attractive material for room-temperature semi-conductor radiation detection due to its high atomic number and density. Performance of better than 1% FWHM at 662 keV has been measured on ∼5 x 5 x 5 mm^3 pixelated TlBr detectors. Though most TlBr detectors show expected performance, a few detectors have high-energy tails on their photopeaks which are caused by non-flat tails on anode waveforms. The properties of these anode tails are studied and the generation of extra electrons by the movement of holes is proposed to explain the observations. The detector is operated in reverse bias (with holes drifting towards the pixelated electrode) to help confirm these observations and a mechanism for correcting preamplifier decay from long collection time digital waveforms is developed and used in the analysis.**

***Index Terms*—TlBr, room-temperature semiconductors, pixelated detectors, preamplifier decay correction.**

I. Introduction

THALLIUM-BROMIDE (TlBr) is being developed as a room-temperature semi-conductor radiation detector due to its high stopping power (large atomic number and density) and favorable crystal properties (simple cubic structure and low melting point). Large volume boules have been grown by the traveling molten zone by multiple researchers [1]-[3]. Performance of better than 1% FWHM at 662 keV has been observed on ∼5 x 5 x 5 mm^3 pixelated TlBr detectors when cooled to $-20°C$ [4], [5].

At room-temperature, TlBr devices fail (or polarize) most likely due to ionic conduction in the material. Previous results have shown the failure of these detectors is due to degredation of the contact material [6]. Improvements in room-temperature lifetime have been achieved by multiple methods including applying Tl electrodes [7] and improved surface preparation [8]. The use of Tl electrodes is undesirable because it requires periodically switching the polarity of the bias [9] which prevents pixelated detectors from operating properly.

Using the best current surface preparation techniques, the lifetime of TlBr detectors have been extended to greater than 100 days at room-temperature [8], [10]. Some of these long-lived TlBr detectors have shown high-energy tails on their photopeaks. This is similar to previously observed high-energy tailing in mercuric-iodide (HgI) where Auger recombintation was proposed to explain the effect [11]. In this work, we investigate the causes of this high-energy tailing by analyzing the digitized waveforms and conclude that there is strong evidence that the cause is charge multiplication by drifting holes. A correction for preamplifier decay for digital waveforms is developed due to the long collection times required in the measurement.

S. O'Neal, Z. He, and C. Leak are with the Department of Nuclear Engineering and Radiological Sciences, Univeristy of Michigan, Ann Arbor, MI, 48109 USA email:onealsp@umich.edu

Manuscript received July 6, 2017; revised August 29, 2017.

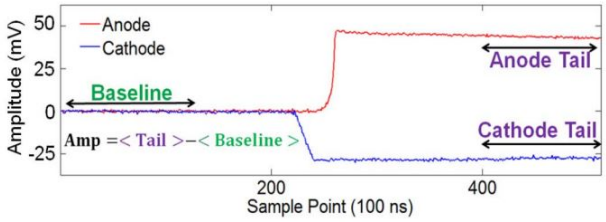

Fig. 1. Example of 100 point simple subtraction.

II. Methods

A. Experimental Setup

The TlBr detector reported in this work was grown by Radiation Monitoring Devices (RMD). The material was purified and grown using the traveling molten zone (TMZ) method and an approximately 5 mm x 5 mm x 5 mm cube was cut from the resulting boule. The material was then etched with HCl and platinum electrodes were deposited by ion-beam at Lawrence Livermore National Lab. More information about the detector fabrication and performance can be found in Ref [10]. The detector has a three-by-three pixelated anode each with a 0.9 x 0.9 mm^2 pixel pad with 1 mm pitch and a planar cathode. A 0.5 mm thick guard ring surrounds all the anode pixels. The signal from each electrode was readout using eV-Products 509 charge-sensitive preamplifiers whose outputs were digitized by 14-bit GaGe Octopus CompuScope PCIe digitizers. For each waveform, 512 samples were recorded at sampling frequencies between 1 MHz and 10 MHz. The detector was cathode-biased to -1000V (unless otherwise noted) and flood irradiated with ^{137}Cs.

B. Digital Pulse Processing

For most TlBr detectors, the amplitudes of each waveform are determined by simple subtraction (see Fig. 1). One-hundred data points are used for both the tail and the baseline region averages. For waveforms which had non-flat tails after the primary charge collection, a modified "prompt subtraction" was used (see Fig. 2). The turning point was determined by a fast shaper, and fifteen points around this turning point were used as the tail amplitude (using the same 100 points as the baseline amplitude). The depth for all waveforms was calculated using the cathode-to-anode-ratio (CAR) [12].

1) Mean Waveform Generation: Mean photopeak anode and cathode waveforms were generated for each pixel in multiple depth windows. The amplitude of each waveform was determined by prompt subtraction and the depth from CAR. Each waveform was then normalized by the anode amplitude, and all waveforms in a CAR bin were averaged. This allowed for the study of the anode and cathode slopes with less noisy waveforms.

This article has been accepted for publication in a future issue of this journal, but has not been fully edited. Content may change prior to final publication. Citation information: DOI 10.1109/TNS.2018.2804165, IEEE Transactions on Nuclear Science

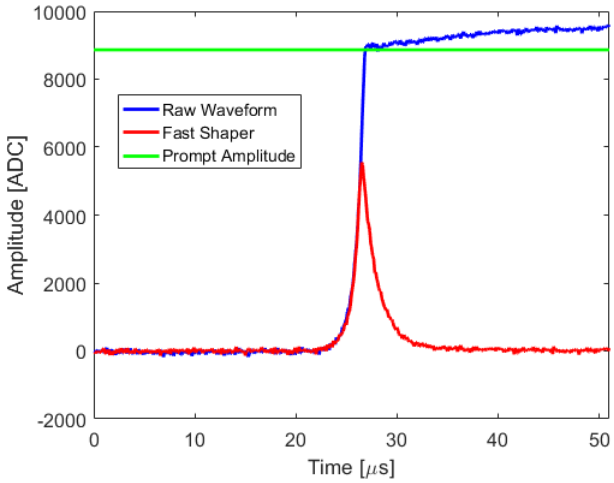

Fig. 2. Example of prompt subtraction shaping. The raw waveform is shown in blue and the fast shaper is shown in red. The horizontal green line shows the amplitude determined from prompt subtraction.

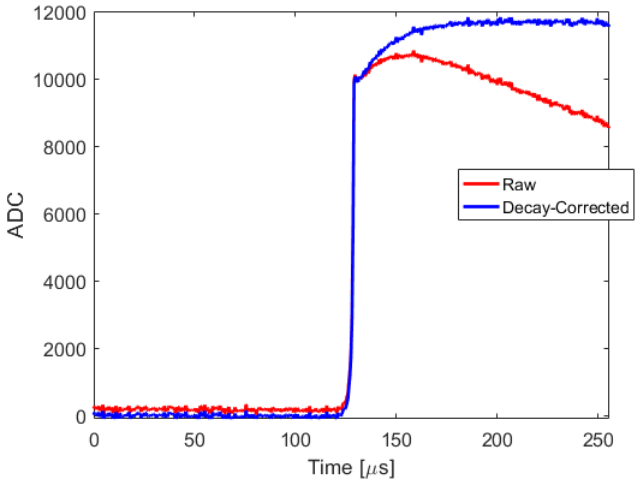

Fig. 3. Example of a raw waveform (shown in red) and after the decay correction (shown in blue). Data was taken at 2MHz.

2) Preamplifier Decay Correction: For some measurements in this work, the sampling window was extended well beyond the normal time, from 512 samples at 10 MHz, or 51.2 μs, to as much as 512 μs in order to fully capture the waveform tails. This caused the waveforms to suffer significant preamplifier decay during the sampling window (see red waveform in Fig. 3). This decay can be modeled as an exponential so the preamplifier output, f(t), from an induced charge, Q_0, at time t = 0 is given by

$$f(t) = Q_0 e^{-t/\tau} \tag{1}$$

where τ is the decay constant. The measured waveform, Q(t), can be expressed as a convolution of this decay function and the rate of charge induction, q(t), or

$$Q(t) = \int_0^t q(\Delta) e^{-\frac{t-\Delta}{\tau}} d\Delta = [q * f](t) \tag{2}$$

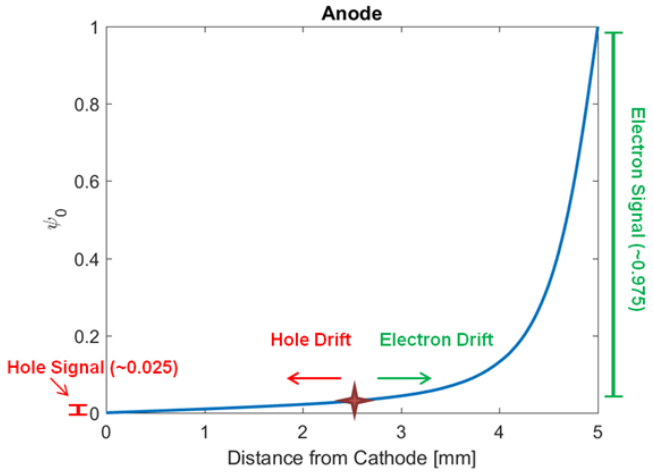

Fig. 4. Anode weighting potential (ψ_0) in the detector and demonstration of the possible signal induction by holes on the anode.

Using the Fourier Transform, the unknown charge induction rate, q(t), can be deconvolved from the measured waveform, Q(t), if the preamplifier decay function is known, or

$$q(t) = \mathcal{F}^{-1}\left\{\frac{\mathcal{F}\{Q(t)\}}{\mathcal{F}\{f(t)\}}\right\} \tag{3}$$

and the undecayed waveform, $Q^*(t)$, can then be constructed by integrating the resulting q(t), simulating a preamplifier with a decay constant of infinity.

$$Q^*(t) = \int_0^t q(t')dt' \tag{4}$$

In discrete space, Eq. 3 can be applied using the discrete-time Fourier Transform (DTFT), and the decay of the preamplifiers can be corrected assuming the decay constant τ is known. Fig. 3 shows an example raw and decay-corrected waveform for data taken at 2 MHz (256 μs collection time). This decay correction was applied to all waveforms in this work using a decay constant determined empirically from flatting the tail of waveforms from another detector which did not show positive anode slopes.

III. Results

Fig. 2 shows a raw anode wavefrom with an anode slope compared to a typical anode waveform shown in Fig. 1. Typically anode waveforms show no rise after the primary charge collection. Sometimes cathode waveforms show a slope after electron collection which is due to hole motion [5]. Due to the weighting potential, the signal on the anode cannot be a result of hole motion unless the holes are generated very close to the anode.

Fig. 4 shows the weighting potential of the anode and demonstrates the small amount of signal that holes can induce on the anode for events in the middle of the detector. This signal is smaller than the observed anode tail. Additionally, Fig. 5 shows this on a measured waveform for another TlBr detector with the same anode geometry, where the cathode shows full collection of holes, but the anode has no slope.

This article has been accepted for publication in a future issue of this journal, but has not been fully edited. Content may change prior to final publication. Citation information: DOI 10.1109/TNS.2018.2804165, IEEE Transactions on Nuclear Science

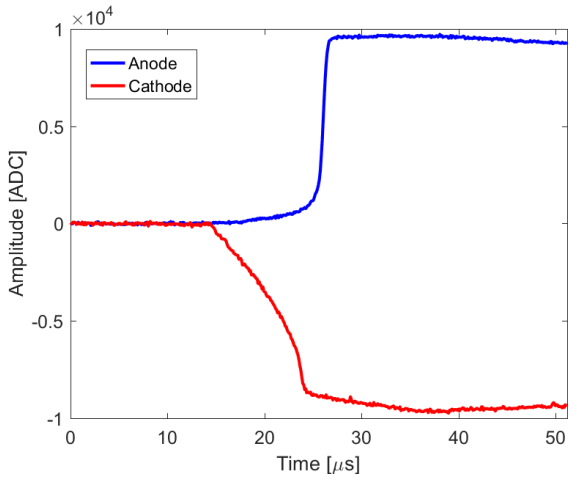

Fig. 5. Example anode (blue) and cathode (red) waveforms for detector 935-35AA1L showing hole motion in the cathode, but no slope on the anode.

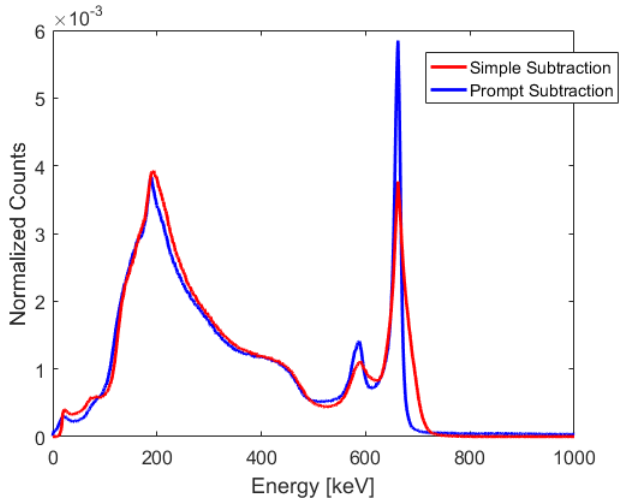

Fig. 6. Depth-corrected spectra for detector 935-38AA2L using both simple subtraction (red) and prompt subtraction (blue) to determine the pulse amplitude. With the removal of the tail, the resolution improves from 4.59% FWHM at 662 keV to 2.21%.

Non-zero anode slopes are observed at all depths, so they cannot be signal induced by holes, therefore they must be caused by electrons which arrive much later than the primary charge cloud.

Fig. 6 shows a comparison of the depth-corrected single-pixel spectrum when the amplitude is determined by simple subtraction and the prompt subtraction method discussed in section II-B. The photopeak has a large high-energy tail when simple subtraction is used. When prompt subtraction technique is used, the charge in the tail of the waveform is ignored and the resolution improves. Furthermore the noise has a higher impact on the prompt subtraction amplitude because only 15 points are used to determine amplitude instead of 100 in the case of simple subtraction. So the improvement of the resolution despite the increase in noise is unexpected.

The improvement in performance indicates the charge in the tail of the waveform is not directly generated by the initial gamma-ray interaction. If it were from the primary event, such as charge that has been delayed by trapping and de-trapping, ignoring this charge should not improve the performance. Therefore the signal in the tail of the anode waveform is extra charge generated by some other process during the drift of electrons and holes.

A. Mean Waveforms

Fig. 7 shows the average (a) anode and (b) cathode waveforms for the cathode side ($0.9 < \text{CAR} < 1.0$), near cathode side ($0.7 < \text{CAR} < 0.85$), middle ($0.45 < \text{CAR} < 0.55$), and anode side ($0.25 < \text{CAR} < 0.35$) of the detector at 2 MHz sampling. In this time window, the full anode charge is collected, but the full cathode signal is only collected in the larger two depth ranges. As shown in Fig. 7(a), the relative amount of extra charge on the anode increases towards the anode side.

Fig. 8 shows a comparison of the average waveforms from the middle of the detector at two different biases (-800V and -1000V). At the higher bias, there is relatively more extra charge. From the results shown in Figs. 7 and 8, two

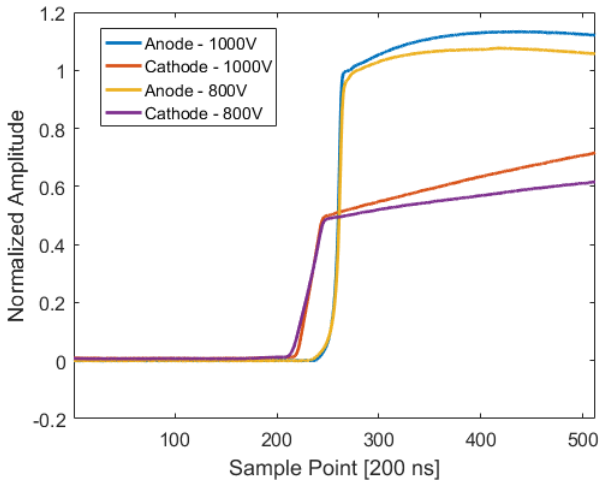

Fig. 8. Comparison of the average waveforms from the middle of the detector at two different biases.

possible explanations for the cause of these anode slopes can be eliminated.

First, if the charge in the anode tail region was caused by trapping and de-trapping of electrons it would increase with electron drift distance (be higher nearer to the cathode side). Also, at the at higher bias, there should be less trapping, so the relative amount of charge in the tail of the waveform should decrease with increasing bias, rather than the observed increase. These observations verify the conclusion drawn from the spectrum (see Fig. 6).

Second, if this extra charge was generated by the drift of the electrons by some other mechanism than trapping, it would likely increase with increasing electron drift distance. This was not observed. Instead, the amount of extra charge increases with increasing hole drift distance. This is shown by both the increasing towards the anode side and the increase with increasing bias, as both of these effects increase the distance

This article has been accepted for publication in a future issue of this journal, but has not been fully edited. Content may change prior to final publication. Citation information: DOI 10.1109/TNS.2018.2804165, IEEE Transactions on Nuclear Science

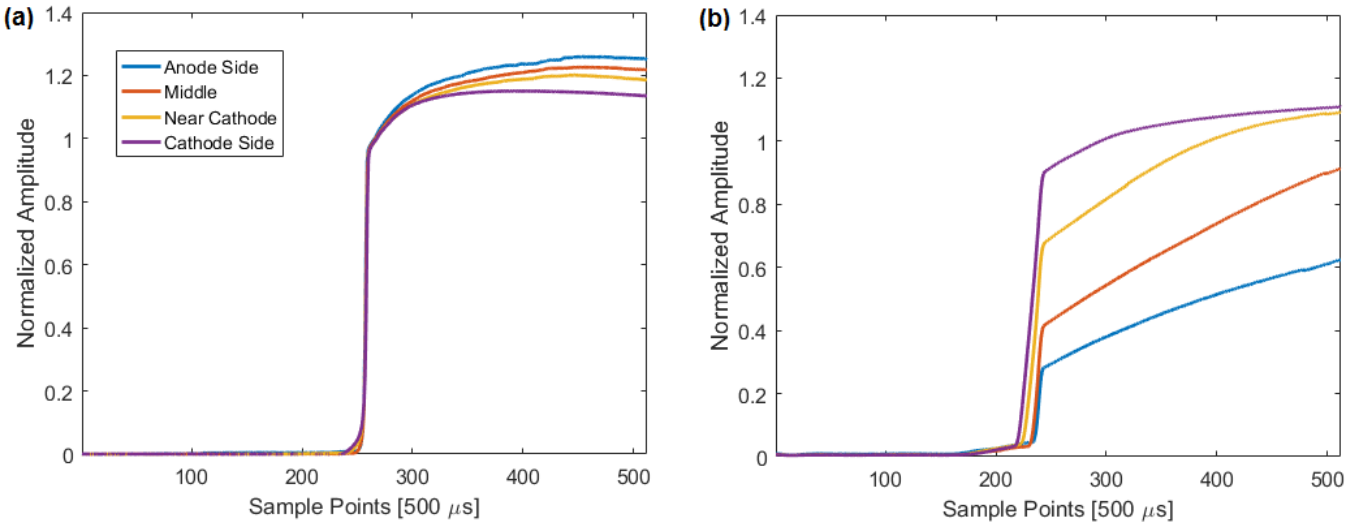

Fig. 7. Mean (a) anode and (b) cathode waveforms for the cathode side, near cathode side, middle, and anode side of detector 935-38AA2L at 1000 V and 2 MHz.

traveled by holes in the collection time.

Therefore, the most consistent explanation for the observed waveform tails is extra charge which originates from holes generating electrons as they drift towards the cathode. Physically this could be caused by Auger recombination as proposed by Gerrish for explaining a similar behavior in HgI [11].

B. Quantification of Extra Charge

Investigation of the characteristics of the anode tails shows that it is likely the drift of holes giving rise to the extra charge, but does not indicate whether the hole must be trapped to free an electron, or if one hole can produce multiple extra electrons. Quantitative investigation of the extra charge can be used to address this question.

This final cathode amplitude is the sum of the signal induced by the electrons, holes, and the extra charge, or

$$C_T = Q_0 + C_{extra} = C_{electron} + C_{hole} + C_{extra} \quad (5)$$

where Q_0 is the initial charge created by the gamma-ray assuming the trapping is negligible. The electron component of the cathode signal is the normalized depth times the initial charge.

$$C_{electron} = \frac{Z}{D} Q_0 \quad (6)$$

Where Z is the depth of interaction and D is the detector thickness. The electron component of the cathode waveform can be estimated using the prompt subtraction shaping method, and from this the signal generated on the cathode by the extra charge can be estimated.

$$C_{extra} = C_T - \frac{D}{Z} C_{electron} \approx C_T - \frac{D}{Z} C_{prompt} \quad (7)$$

Where C_{prompt} is the cathode amplitude calculated by prompt subtraction. The signal from the extra charge on the anode can similarly be estimated by subtracting the prompt shaped amplitude from the final anode amplitude.

$$A_{extra} = A_T - A_{prompt} \quad (8)$$

TABLE I
ESTIMATED SIGNAL FROM EXTRA CHARGE ON ANODE AND CATHODE

				Extra Charge	
CAR Range	Mean Z/D	C_T	C_{prompt}	C_{extra}	A_{extra}
0.9-1.03	0.965	1.083	0.942	0.107	0.156
0.7-0.85	0.775	1.067	0.704	0.158	0.239

TABLE II
COMPARISION OF ESTIMATED AND MEASURED CATHODE SIGNAL FROM EXTRA CHARGE

	Measured	Predicted		Measured
CAR Range	A_{extra}	C_{extra1}	C_{extra2}	C_{extra}
0.9-1.03	0.159(25)	0.153(24)	0.156(12)	0.133(27)
0.7-0.85	0.218(40)	0.169(31)	0.194(20)	0.175(43)

Table I shows the estimated signal from the extra charge on both the anode and cathode for the two fully collected cathode waveforms from Fig. 7. As previously stated, the amount of extra charge decreases with increasing electron drift distance. Also, the signal on the cathode is less than the signal on the anode. This is expected as the cathode extra charge can be expressed as the average drift distance times the anode extra charge.

$$C_{extra} \approx \frac{\bar{Z}}{D} A_{extra} \quad (9)$$

Where $\bar{Z}$ is the mean depth at which the extra charge is generated. Table II shows a comparison of the measured cathode extra charge to the predicted cathode extra charge (calculated using Eq. 9) under two different assumptions.

C_{extra1} assumes the extra charge is generated at the same location as the primary charge and C_{extra2} assumes the charge

This article has been accepted for publication in a future issue of this journal, but has not been fully edited. Content may change prior to final publication. Citation information: DOI 10.1109/TNS.2018.2804165, IEEE Transactions on Nuclear Science

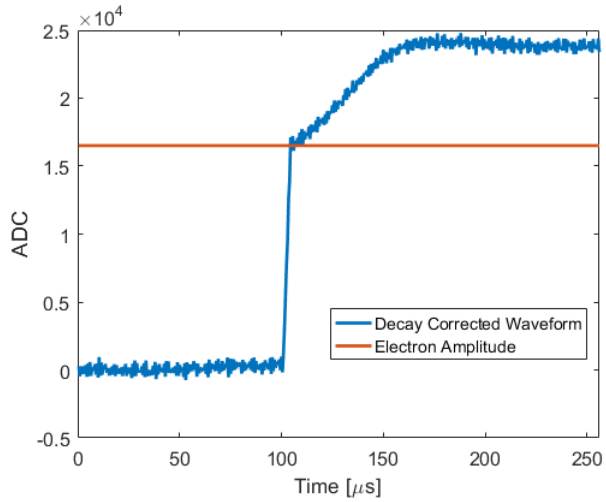

Fig. 9. Planar electrode waveform in positive bias (+2000V), with the red line showing the amplitude from electrons determined by prompt subtraction.

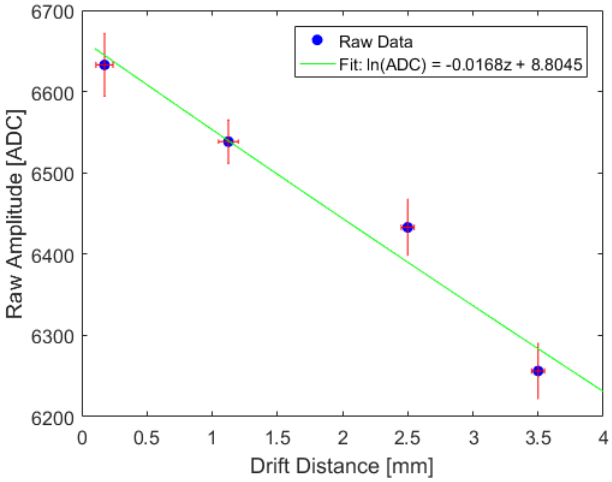

Fig. 10. Trapping on planar electrode (holes) in reverse bias (+2000V) with an exponential fit.

is generated uniformly along the drift of the holes towards the cathode. The measured and predicted values for C_{extra} do not differ beyond uncertainty. Due to the high uncertainty in these values, no conclusion can be made about which charge generation model is more appropriate. Due to the close agreement between the measured and predicted cathode extra charge, we cannot conclude from this data whether the holes have to be trapped to free an electron, or if one hole can generate more than one electron.

C. Positive Bias

To determine if holes have to be trapped in order to free an electron (thus requiring a one to one conversion) the hole trapping was estimated by operating the detector in positive bias. Under positive bias, the holes drift towards the pixelated electrode. Fig. 9 shows an example planar electrode waveform under positive bias. The planar electrode has contributions from both electrons and holes, with the initial fast rise due to electrons. Prompt subtraction was used to estimate the electron only component of the planar electrode waveform, so that the depth could be estimated using a modified CAR.

$$\frac{Z}{D} = \frac{Electron\ Planar\ Component}{Pixelated\ Amplitude} \tag{10}$$

Fig. 10 shows the pixel amplitude (hole signal) versus drift distance as calculated by Eq. 10. The expected signal amplitude, N, versus depth is given by Eq. 11 [13].

$$N = N_0 e^{-\mu\tau z/E} \tag{11}$$

The data is fit using Eq. 11 and the $(\mu\tau)_h$ was estimated to be $1.49\times10^{-3}\ cm^2/(Vs)$. Using this estimate of the $(\mu\tau)_h$, the trapping of holes in the fully collected waveforms shown in Fig. 7 can be estimated. Table III shows a comparison of this estimated hole trapping with observed anode extra charge. Not enough holes are trapped to account for the amount of extra charge observed on a one-for-one basis, therefore it must not be necessary for the hole to be trapped in order to free an electron.

TABLE III
COMPARISON OF ESTIMATED HOLE TRAPPING AND ANODE EXTRA CHARGE

CAR Range	Predicted Hole Trapping	Relative Anode Extra Charge
0.9-1.03	0.003	0.156
0.7-0.85	0.0187	0.239

IV. CONCLUSION

Delayed charge collection has been observed on anode waveforms in TlBr detectors resulting in high-energy tails on photopeaks. Through digital signal processing, this delayed charge can be ignored and the detector performance improves, indicating this charge is not from the primary gamma-ray interaction. The amount of observed extra charge is correlated to hole drift distance and is therefore likely generated from the drift of holes.

By operating the detector in reverse bias, the $(\mu\tau)_h$ was estimated. The amount of hole trapping is not equal to the amount of observed extra charge on the anode, therefore it is likely that the holes can generate extra electrons through drifting without requiring trapping. The exact mechanism for this release of extra charge is unknown at this time and limited to only a few TlBr detectors.

ACKNOWLEDGMENT

The authors would like to thank Leonard Cirinagno, Hadong Kim, and Kanai Shah at RMD, Inc. for growing the detector presented in this work, and also Adam Conway at LLNL for the etching and electrode deposition. This work was funded by DNDO of DHS under a subcontract through Radiation Monitoring Devices (Contract #HSHQDN-16-C-00024)

REFERENCES

[1] A. V. Churilov, W. M. Higgins, G. Ciampi, H. Kim, L. J. Cirignano, F. Olschner, and K. S. Shah, "Purification, crystal growth and detector performance of TlBr," *Proc. SPIE*, vol. 7079, p. K1-K8, 2008.

[2] H. Kim, L. Cirignano, A. Churilov, G. Ciampi, W. Higgins, F. Olschner, and K. Shah, "Developing larger TlBr detectors: Detector performance," $IEEE\ Trans.\ Nucl.\ Sci.$, vol 56, no.3, 2009.

[3] K. Hitomi, T. Onodera, T. Shoji, and Z. He, "Pixellated TlBr detectors with the depth sensing technique," $Nucl.\ Instr.\ Meth.\ A$, vol. 578, pp. 235-238, Jul. 2007.

[4] C. Thrall, W. Kaye, Z. He, H. Kim, L. Cirignano, and K. Shah "Transient behavior in TlBr gamma-ray detectors and its analysis using 3-d position sensing" $IEEE\ Trans.\ Nucl.\ Sci.$, vol 60, no. 2, 2013.

[5] W. Koehler "Thallium Bromide as an Alternative Material for Room-Temperature Gamma-Ray Spectroscopy and Imaging " Ph. D. Thesis, University of Michigan, 2014.

[6] W. Koehler, Z. He, C. Thrall, S. O'Neal, H. Kim, L. Cirignano, and K. Shah "Quantitative investigation of room-temperature breakdown effects in pixelated TlBr detectors" $IEEE\ Trans.\ Nucl.\ Sci.$, vol 60, no. 2, 2013.

[7] K. Hitomi, T. Shoji, and Y. Niizeki, "A method for suppressing polarization phenomena in TlBr detectors," $Nucl.\ Instr.\ Meth.\ A$, vol. 585, pp. 102-104, Jan. 2008.

[8] A. Conway, L. Voss, A. Nelson, P. Beck, T. Laurence, R. Graff, R. Nikolic, S. Payne, H. Kim, L. Cirignano, and K. Shah, "Fabrication methodology of enhanced stability room temperature TlBr gamma detectors" $IEEE\ Trans.\ Nucl.\ Sci.$, vol 60, no. 2, 2013.

[9] K. Hitomi, Y. Kikuchi, T. Shoji, and K. Ishii. "Improvement of energy resolutions in TlBr detectors." $Nucl.\ Instr.\ Meth.\ A$, vol. 601, pp. 112-115, Aug. 2009.

[10] S. O'Neal, W. Koehler, Z. He, H. Kim, L. Cirignano, K. Shah, A. Conway, E. Swanberg, L. Voss, R. Graff, A. Nelson, and S. Payne, "Improvements in room temperature lifetime of pixelated TlBr detectors from surface etching," $2015 IEEENSS/MIC$, San Diego, CA, 2015.

[11] V. Gerrish, "Polarization and gain in mercuric iodide gamma-ray spectrometers," $Nucl.\ Instr.\ Meth.\ A$, vol. 322, pp. 402-413, Nov. 1992.

[12] Z. He, W. Li, G. Knoll, D. Wehe, J. Berry, and C. Stahle, "3-d Position sensitive CdZnTe gamma-ray spectrometers" $Nucl.\ Instr.\ Meth.\ A$, vol. 442, no.13, pp. 173-198, 1999.

[13] Z. He, G. Knoll, and D. Wehe, "Direct measurement of product of the electron mobility and mean free drift time of CdZnTe semiconductors using position sensitive single polarity charge sensing detectors," $J.\ App.\ Phys.$, vol. 84, no. 10, 1998.